

Enhanced photocatalysis performance of BiOCl/graphene modified via polyvinylpyrrolidone

F.Q. Li^a, B.H. Sun^{a,b}, Y.L. Qin^{a,b,*}, X.Y. Liu^{a,b}, Z.Y. Liu^{b,**}, D.R. Ni^b, B.L. Xiao^b, Z.Y. Ma^b

^a School of Science, Shenyang Ligong University, No.6 Nanping Central Road, Shenyang, 110159, China

^b Shi-changxu Innovation Center for Advanced Materials, Institute of Metal Research, Chinese Academy of Sciences, 72 Wenhua Road, Shenyang, 110016, China

ARTICLE INFO

Keywords:
BiOCl
Graphene
Hydrothermal
Photocatalysis

ABSTRACT

With the aim to improve the photocatalytic property, BiOCl/graphene (BR) and BiOCl/graphene modified via polyvinylpyrrolidone (BRP) were prepared in a hydrothermal route. The obtained BRP sample showed the highest photocatalytic activity for the degradation of Methyl Orange (MO) under visible light illumination as compared to the pure BiOCl and BR samples. The results indicate that the degradation rate constant of the BR reached 0.04874 min^{-1} as compared to the 0.03227 min^{-1} for the pure BiOCl. It was found that the reduced graphene oxide (RGO) could uniformly load BiOCl, and the chemical bonding interface between RGO and BiOCl reduced the recombination of electron-hole pairs. Further, adding polyvinylpyrrolidone could refine the size of the BiOCl and increase the number of the BiOCl adhered onto the graphene surface, and thereby providing the highest efficient catalytic effect, with the degradation rate constant reaching 0.06205 min^{-1} .

1. Introduction

Environmental pollution and energy shortages become the focus of world attention. The problem of environmental pollution is mainly the air pollution, water pollution, and solid pollution. Among these three kinds of pollution, water pollution is the most relevant to our daily life and also the most extensive one. Semiconductor photocatalysis is one of the most promising solutions for water pollution [1–5]. The semiconductor photocatalyst is irradiated by sunlight, generating photoelectrons and photoholes. These electrons and holes can transfer to the surface of photocatalyst and generate a series of reduction-oxidation with water and oxygen molecules, degrading the organic molecules adsorbed on the surface of the photocatalyst [6].

In recent years, as a novel ternary oxide semiconductor, BiOCl has attracted great attention for its excellent photocatalytic performance [7–9]. Nevertheless, BiOCl has two fatal defects. One is that pure BiOCl limits the photocatalytic activity in sunlight due to its large indirect bandgap in the range of 3.02–3.5 eV [10]. The other is that the rapid recombination of light-induced electrons and holes greatly reduces the quantum efficiency [11].

So far, various strategies have been used to overcome these defects, such as composite semiconductors, doping, precious metal deposition,

and morphology control. Among these methods, the combination of semiconductor and graphene to prepare two-dimensional structure photocatalysis has become a research hotspot in recent years. Graphene has good conductivity and large specific surface area, and this can not only effectively separate electrons-holes but also increase the adsorption capacity of organic pollutants and photocatalytic active sites, thereby improving the efficiency of the photocatalytic reaction greatly [12].

Graphene owns a 2D carbon network formed by sp^2 hybridization and attracts much interest because of its unique electrical properties, such as high electron mobility, high specific surface area [6,13–16]. Owing to these advantages, the photocatalytic performance of the photocatalyst/graphene nanocomposites can be improved. Reduced graphene oxide (RGO) is the most commonly used precursor of graphene due to its abundant surface functional groups. Now there are some researches on the list of photocatalyst/RGO nanocomposites, such as ZnS/RGO [13], BiOCl/RGO [14], CdS/RGO [17], TiO_2 /RGO [18], etc. So, the preparation of BiOCl/RGO nanocomposites can further improve the photocatalytic performance of pure BiOCl. However, few researches have focused on how to control particle size and achieve better dispersion of BiOCl.

In this study, pure BiOCl were synthesized via the solvothermal method, and BiOCl/RGO nanocomposites were synthesized via the

* Corresponding author. School of Science, Shenyang Ligong University, No.6 Nanping Central Road, Shenyang, 110159, China.

** Corresponding author.

E-mail addresses: qylndr0628@163.com (Y.L. Qin), zyliu@imr.ac.cn (Z.Y. Liu).

<https://doi.org/10.1016/j.vacuum.2020.109857>

Received 24 August 2020; Received in revised form 15 October 2020; Accepted 16 October 2020

Available online 24 October 2020

0042-207X/© 2020 Elsevier Ltd. All rights reserved.

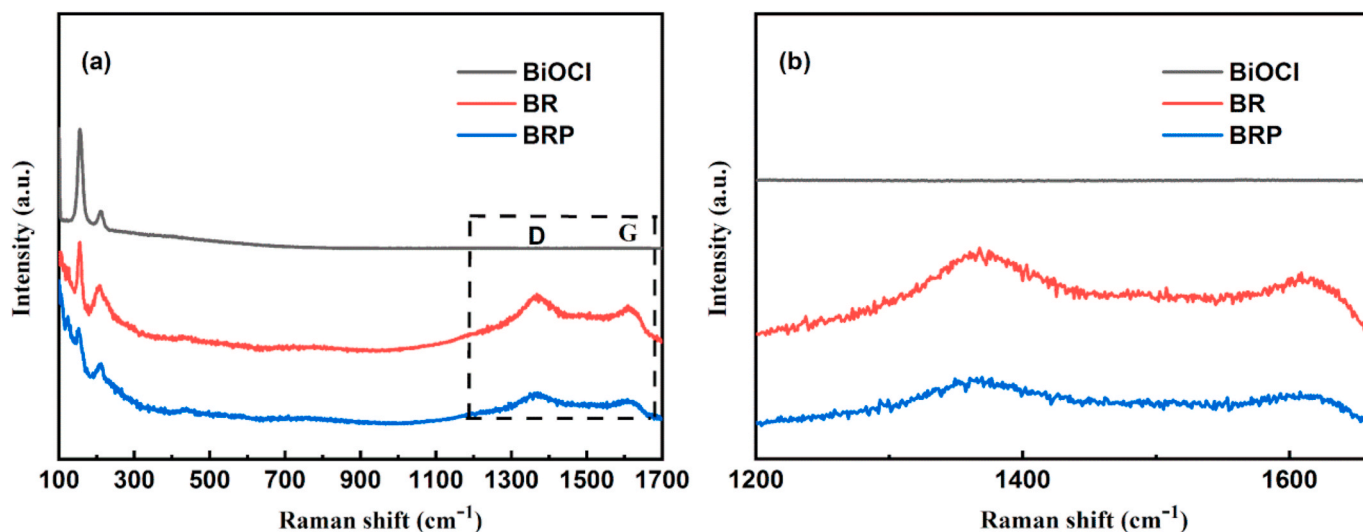


Fig. 1. (a) Raman spectrum of prepared samples, (b) magnified view of RGO in (a).

hydrothermal method with GO aqueous solution as the precursor. Then polyvinylpyrrolidone (PVP) was added in the synthesis process of BiOCl/RGO-PVP nanocomposites, and the influences of PVP on the morphology of the composites were studied. Besides, the photocatalytic properties of the pure BiOCl and two composites were evaluated by photodegrading methyl orange (MO) under visible light exposure for comparison.

2. Experimental

2.1. Preparation

2.1.1. Solvothermal preparation of BiOCl

Typically, 3 mmol $\text{Bi}(\text{NO}_3)_3 \cdot 5\text{H}_2\text{O}$ was dissolved in 20 ml the glycol solution by constant stirring. Additionally, 3 mmol KCl and 1 mmol citric acid were dissolved in 20 ml the glycol and deionized water (1:1) solution followed by constant stirring. After 30 min stirring, the KCl solution was gradually added to the $\text{Bi}(\text{NO}_3)_3 \cdot 5\text{H}_2\text{O}$ solution, and the mixture was then kept stirring for another 30 min at room temperature. The resulting solution was transferred to a 100 ml stainless steel autoclave, treated at 120 °C for 12 h, and then cooled to room temperature. The sample was centrifuged, washed several times with distilled water and ethanol, and dried at 80 °C. Finally, the photocatalyst was ground to powder, and the pure BiOCl samples were obtained.

2.1.2. Preparation of BiOCl/graphene composites

0.01 g graphene oxide (GO) was dispersed in 10 ml ethanol and 20 ml deionized water and then sonicated for 30 min. Thereafter, 0.2 g BiOCl was added to the above reaction mixture, followed by magnetic stirring for 2 h. The mixture was then transferred to a 100 ml polytetrafluoroethylene-lined stainless steel autoclave and heated at 160 °C for 3 h. After naturally cooling to room temperature, the obtained product was collected and washed thoroughly with deionized water, and then washed with anhydrous ethanol. Finally, the sample was dried at 80 °C for 4 h to obtain BiOCl/RGO. The obtained BiOCl/RGO was represented as BR. Additionally, 0.01 g GO and 0.1 g polyvinylpyrrolidone (PVP) were dispersed in 10 ml ethanol and 20 ml deionized water, followed by sonication for 30 min to obtain BiOCl/RGO-PVP. For comparison, BiOCl/RGO-PVP was also prepared using the same procedure. The obtained BiOCl/RGO-PVP was represented as BRP.

2.2. Characterization

Raman spectrum was used to analyze the chemical structure of the

samples. X-ray powder diffraction (XRD) measurement of the samples was performed using a German Bruker X-ray diffractometer equipped with $\text{Cu K}\alpha$ radiation ($\lambda = 1.541874 \text{ \AA}$). The X-ray photoelectron spectroscopy (XPS) (VG Multilab 2000X, Vacuum Generators, UK) was used to investigate the chemical compositions and the molecular structure of constituent elements. The X-ray source was Mg $\text{K}\alpha$ and the size of the analyzed sample area was 500 μm . The base pressure during the analysis was $3.0 \times 10^{-8} \text{ Pa}$. Prior to analysis, the sample was not etched by Ar^+ . It should be noticed that C 1s method based on adventitious carbon used to be a conventional method to reference XPS spectra [19–21]. In recent years, however, it was reported that the common C 1s method had certain risks and might lead to unphysical results [22–24]. Greczynski et al. [25] pointed out that the method based on the measurement of sample work function should be used to replace the conventional C 1s method in order to avoid risks. However, in our case the work function could not be well measured using ultraviolet photoelectron spectroscopy (UPS), because the samples could not effectively conduct electricity and the bias voltage could not be effectively applied for the equipment. Thus, the conventional method was adopted by setting C 1s peak at 284.6 eV. For this reason results should be treated with the highest degree of caution. The morphology and structural characteristics of the samples were examined by field emission electron microscopy (FE-SEM, SUPRA 55), and the accelerating voltage was 15 kV. Transmission electron microscopy (TEM, FEI Tecnai F20, FEI CO, USA) analysis was performed to characterize the morphology and crystal structure of the samples, and the applied acceleration voltage of TEM was 200 kV.

2.3. Photocatalyst activity measurement

The photocatalytic activity of the prepared samples was evaluated by monitoring the photocatalytic degradation of MO aqueous solution under visible light irradiation 25 cm above the beaker. The prepared photocatalyst (30 mg) was dispersed in a glass vessel containing 50 ml of MO aqueous solution (20 mg/L). The suspension was magnetically stirred in the dark for 30 min before light irradiation to achieve an adsorption-desorption balance between the photocatalyst and MO. Then, 4 ml of the suspension was taken every 10 min during the irradiation and centrifuged for 5 min. The speed of the centrifuge was 10,000 rpm. The centrifuged solution was recorded at its maximum absorption wavelength.

In addition, the photocatalytic activity of the catalyst samples was also evaluated by comparing the apparent reaction rate constants (k). The k could be calculated as: $k = (1/t) \cdot \ln(C_0/C)$, where k is the apparent reaction rate constant, C_0 and C is the initial concentration and

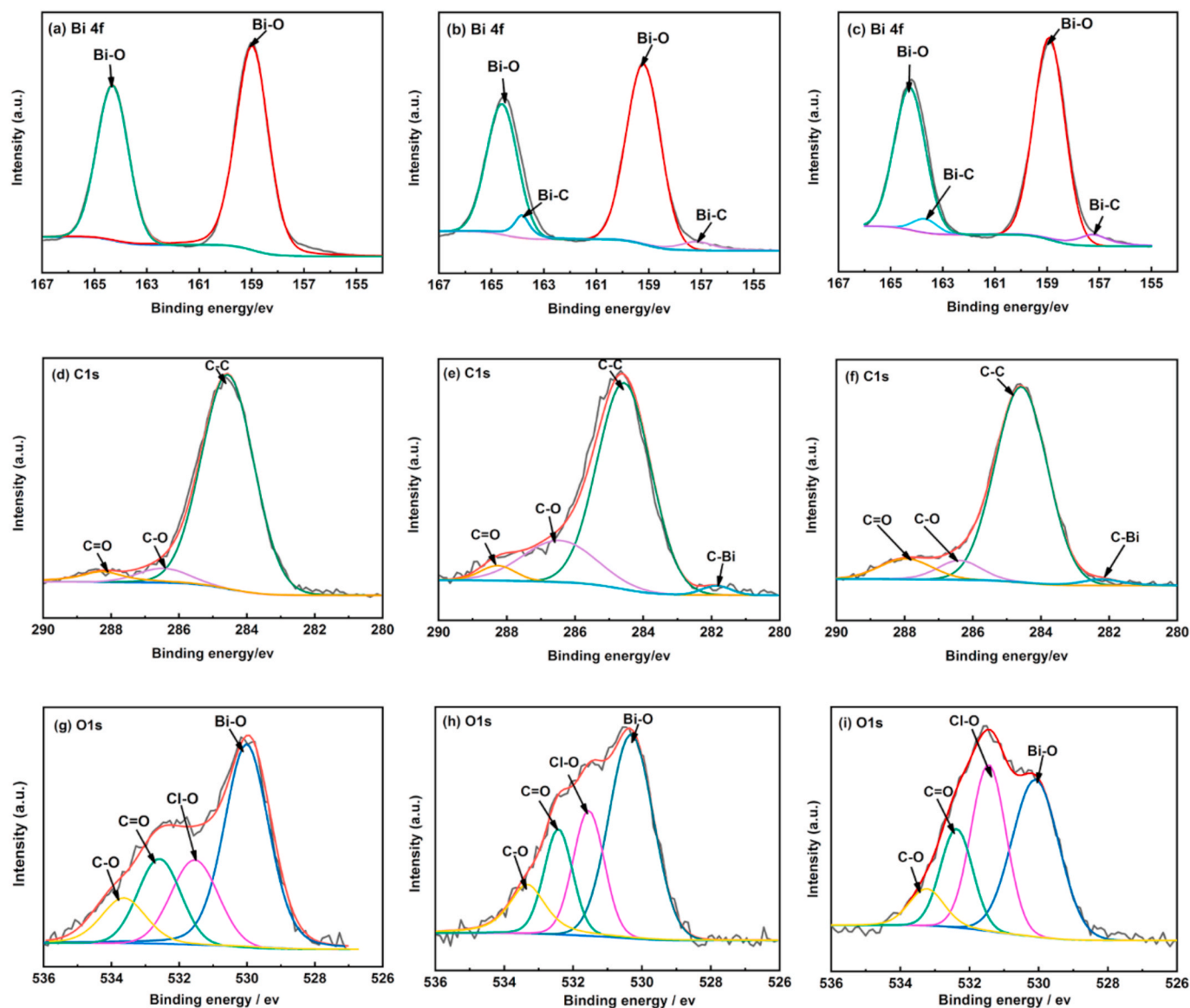


Fig. 2. XPS spectra: (a, b, c) Bi 4f of BiOCl, BR, and BRP, (d, e, f) C 1s of BiOCl, BR, and BRP, (g, h, i) O 1s of BiOCl, BR, and BRP.

the reaction concentration of MO solution, respectively.

3. Results and discussion

3.1. Phase and structure analysis

Raman spectra of BiOCl, BR, and BRP are shown in Fig. 1. As can be seen (Fig. 1a), there were two characteristic peaks occurred at 155 cm^{-1} , and 211 cm^{-1} for the BiOCl sample. For BR and BRP samples (Fig. 1b), RGO with obvious D and G peaks could be detected besides the BiOCl peaks, indicating the existence of RGO and BiOCl. The D peak at 1369 cm^{-1} represents the SP^3 hybrid structure or the SP^2 bond hybrid defect graphene edge structure as crystal defects and disorder induction. The G peak (1614 cm^{-1}) is generated by the stretching motion of all SP^2 atom pairs in the carbon ring or long-chain [26]. It is noteworthy that BR and BRP samples showed wider and weaker peaks of BiOCl, indicating a decrease in crystallinity during the formation of BiOCl complexes [27].

Fig. 2a shows the spectrum of Bi 4f, in which the two peaks of pure BiOCl at 159.06 eV and 164.26 eV assigned to Bi $4f_{7/2}$ and Bi $4f_{5/2}$, respectively, indicating the existence of Bi-O bonds [28,29]. In addition, in Fig. 2b and c BR and BRP showed two small peaks at 163.93, 157.33,

and 163.74, 157.30, respectively. It is believed that the C-Bi bond formed on the GO surface changed the chemical environment of Bi [30]. Because the ability of C to get electrons from Bi was much weaker than that of O, the binding energy of Bi-C shifted to a lower peak than that of Bi-O bond.

Fig. 2d, e, f show the characteristic peaks of C 1s in BiOCl BR and BRP. The C 1s peaks of BiOCl were located at 284.6, 286.4, and 288.32 eV, corresponding to C-C, C-O, and C=O, respectively. The C 1s peaks of BR were located at 284.6, 286.46, and 288.26 eV, corresponding to C-C, C-O, and C=O, respectively. The C 1s peaks of BRP were located at 284.6, 286.39, and 288.10 eV, corresponding to C-C, C-O, and C=O, respectively. However, the strength of C-O and C=O groups containing oxygen was particularly weak. The results showed that the most of the oxygen-containing groups on graphene oxide were reduced in the process of material synthesis [31,32]. A small peak was found at about 281.9 eV in Fig. 2e and f, indicating the existence of C-Bi bonds in the composite system [33]. It can be seen that the formed C-Bi chemical bond replaced the oxygen-containing group on GO, which further reduced GO and increased the proportion of sp^2 -hybrid C atom, which could increase the electron mobility on graphene [34]. In Fig. 2g, h, i, the O 1s core-level spectrum of BiOCl, BR, and BRP all showed a peak

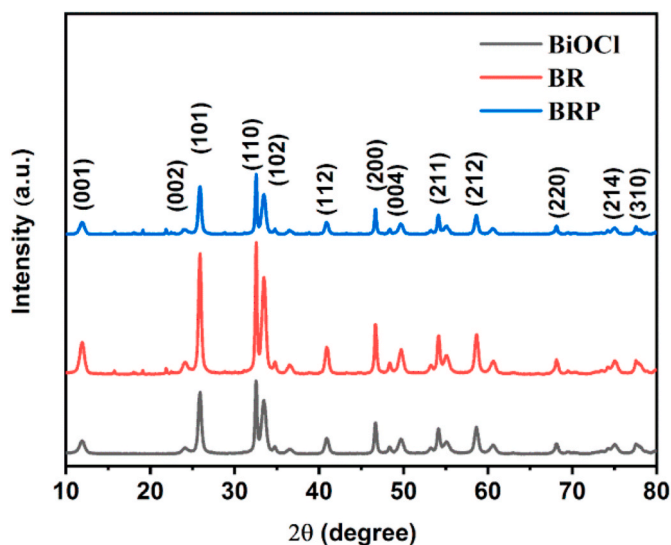


Fig. 3. XRD pattern of the three different composite samples.

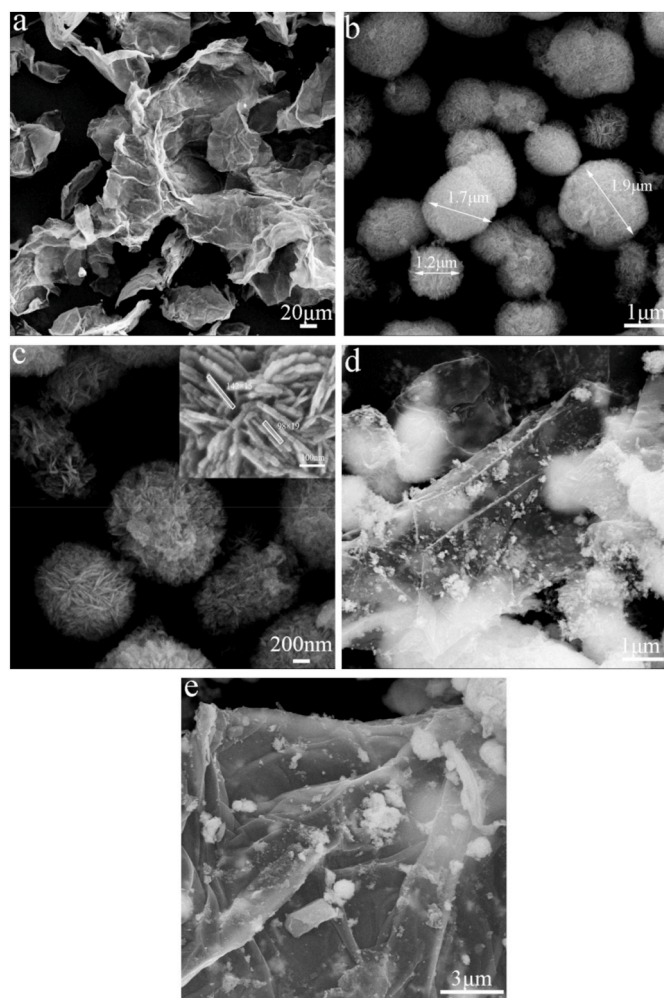


Fig. 4. SEM images of prepared samples: (a) GO, (b, c) BiOCl, (d) BR and (e) BRP.

with a binding energy of about 530 eV, which were related to Bi–O bond. The peak positions are about 531.5, 532.4 and 533.7 eV, corresponding to the Cl–O, C=O and C–O in XPS.

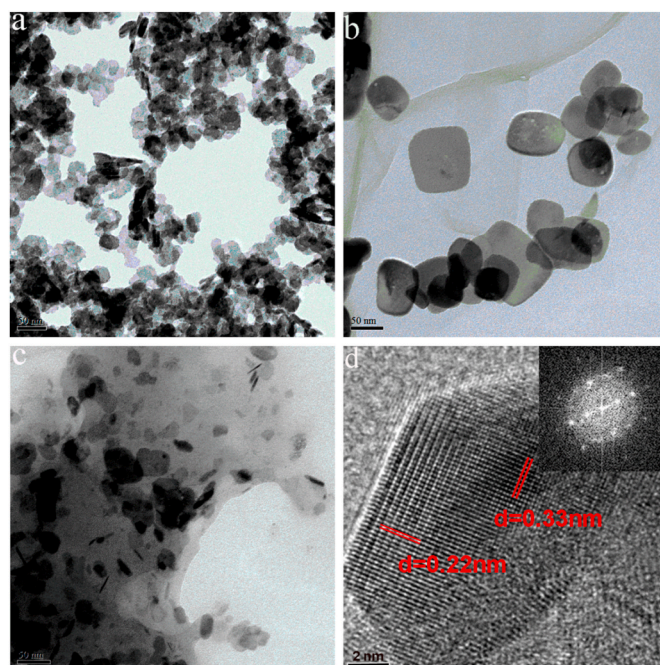


Fig. 5. TEM (a) BiOCl, (b) BR and (c) BRP; (d) HRTEM of BiOCl in BRP, the insert is the FFT of SAED pattern.

The XRD patterns of as-prepared a series of pure BiOCl, BR and BRP, composite are shown in Fig. 3. (001), (002), (101), and (110), etc were the characteristic crystal planes of BiOCl. The diffraction peaks of all the samples were basically the same, Therefore, adding graphene did not change the crystalline phase of BiOCl [35]. It is known that the typical peak value of RGO is at $2\theta = 26^\circ$. However, it is noteworthy that only single-phase BiOCl peaks appeared in the pattern of the composites, and no diffraction peak of RGO could be observed. This is because the content of RGO was too small to be detected [36,37].

3.2. Microscopic morphology analysis

SEM image of GO in Fig. 4a shows that the GO flakes are covered with folds, indicating the small thickness of the GO. For BiOCl in Fig. 4b, the SEM images clearly show that the fabricated BiOCl samples were 3D flower-like microspheres, and the diameters of regular spheres were about 1.2–2.1 μm . The magnified image in Fig. 4c indicates that the microspheres were self-assembled by many smaller sheets.

In Fig. 4d, after GO was added to the reaction system, BiOCl samples were no longer uniformly spheres and many dispersed BiOCl could be observed on the RGO. This could be due to the interaction between the oxygen functional groups and the hydroxyl groups of RGO, which firmly bonded BiOCl. However, many large BiOCl microspheres could still be observed. Fig. 4e shows that the morphology of the BiOCl changed after adding PVP. The number of large microspheres decreased a lot, and more BiOCl were dispersed on the RGO, proving that PVP played a role in preventing polymerization.

TEM images in Fig. 5 agree well with the SEM results shown in Fig. 4. For the pure BiOCl sample (Fig. 5a), the dispersed BiOCl was observed and exhibited obvious aggregation. It should be noted that the BiOCl was vibrated in alcohol by ultrasonic and fished out by copper net when making the TEM sample, which could destroy the 3D flower-like morphology of BiOCl. Therefore, the BiOCl in the TEM image was no longer the perfectly uniform 3D flower-like sphere.

For the BR sample (Fig. 5b), many BiOCl were distributed on the RGO. BR showed a well-ordered structure, which indicates that RGO was beneficial to crystal growth. For the BRP sample (Fig. 5c), the number of BiOCl adhered to the surface of RGO layer increased significantly.

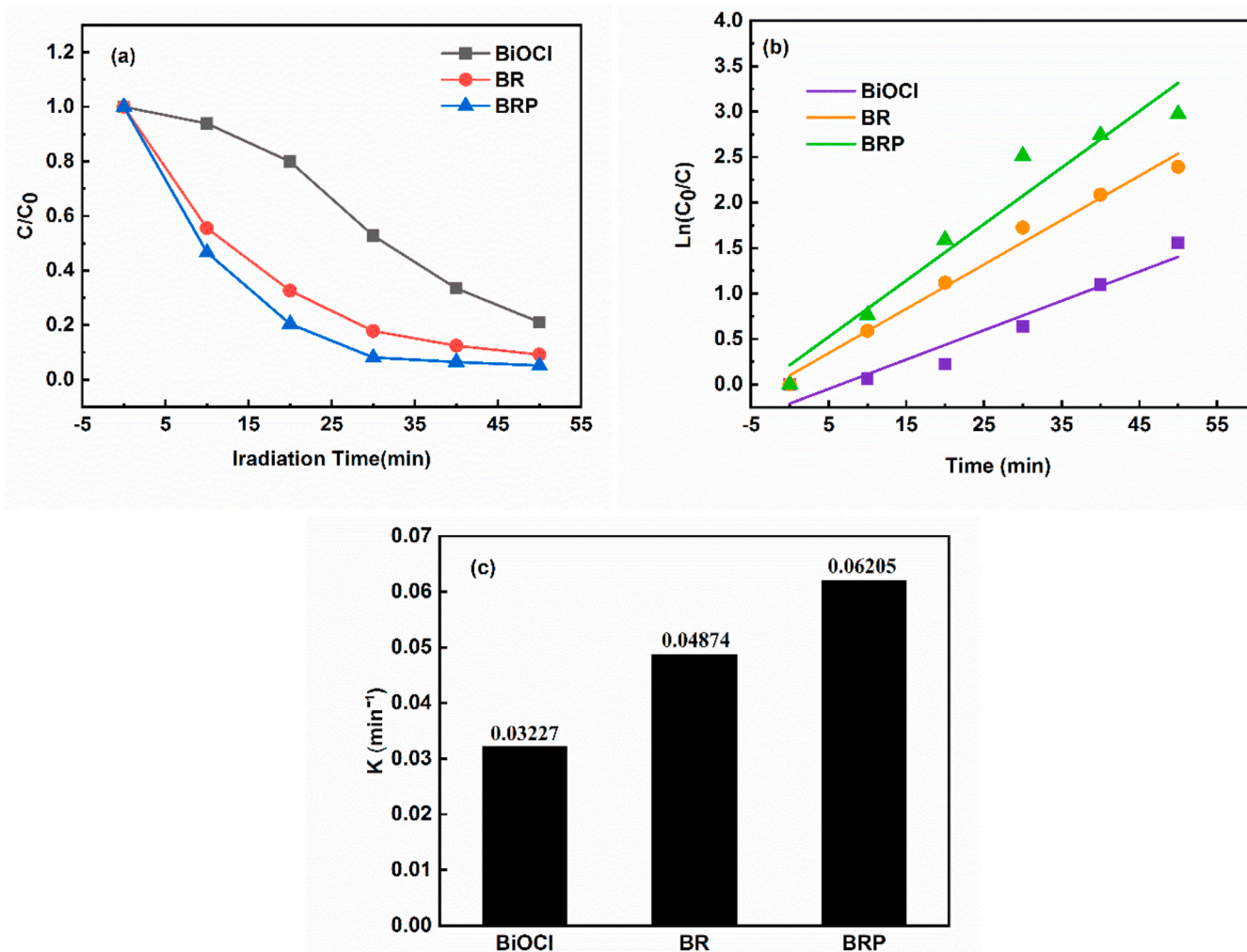


Fig. 6. (a) Photodegradation of MO by BiOCl, BR, BRP, (b) and (c) MO different catalyst photodegradation and quasi-first-order kinetic data quasi-first-order rate constants (k).

Table 1
Photocatalytic kinetic parameters of prepared materials.

Sample	Rate constant (min ⁻¹)	Degradation rate (%)
BiOCl	0.03227	78.9
BR	0.04874	90.9
BRP	0.06205	94.9

Further, the size of BiOCl was smaller and more uniform than those in the BR sample. This indicates that adding PVP could refine the size of BiOCl and inhibit their agglomeration. Fig. 5d showed the corresponding HRTEM image of BiOCl. Several lattice stripes with different lattice distances of 0.33 nm and 0.22 nm were observed clearly, which could be attributed to the (101) and (112) planes of tetragonal BiOCl.

3.3. Characterization of photocatalytic activity

The photocatalytic properties of MO degradation via the prepared samples were tested in the presence of visible light, and the MO concentration of different composites as a function of irradiation time are shown in Fig. 6a, and the degradation rates are also listed in Table 1. The test indicates that the degradation of MO via pure BiOCl was slow, and the degradation rate of pure BiOCl was only 78.9% in 50 min. For BR sample, the degradation rate of MO increased to 90.9% as illumination was performed for 50 min. By comparing, BRP exhibited the highest

photocatalytic performance in the three samples, and its degradation rate reached 94.9% in 50 min.

This could explain as follows. On one hand, a lot of contaminant molecules could adsorb on the surface of RGO, accelerating the degradation efficiency. On the other hand, RGO could prevent the polymerization of BiOCl and relax the agglomeration, thereby increasing the efficiency of photo-generated carriers. Therefore the visible light photocatalytic activity: BR > BiOCl. The addition of PVP could refine the size of BiOCl and increase the number of BiOCl adhered onto RGO surfaces. Therefore the visible light photocatalytic activity: BRP > BR.

The photocatalytic degradation of MO by the nanocomposites under visible light obeyed pseudo-first-order kinetics concerning the concentration of MO:

$$\ln \left(\frac{C_0}{C} \right) = k \times t$$

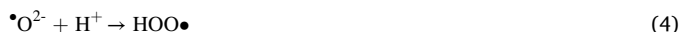
where C and C_0 are the concentration at irradiation time t and the initial time, respectively; k is the degradation rate constant. The photo-degradation linear plots of $\ln(C_0/C)$ vs. t (time) for MO are shown in Fig. 6b, and the calculated values of k are shown in Fig. 6c and Table 1. It is noted that the degradation rate constant (k) of BRP was 0.06205 min⁻¹, which was much higher than other samples.

Based on the above analysis, it can be seen that adding graphene sheet as the support material for the BiOCl catalyst could enhance the

photocatalytic activity. It also shows that the proper addition of PVP during the synthesis process could further improve the photocatalytic activity.

3.4. Photocatalytic mechanism

BiOCl receives a certain amount of external energy and photocatalytic degradation of MO, that is, the external energy of the electron receivers located on the BiOCl conduction band is stimulated to the valence band. The resulting electron-hole pairs can produce active free radicals with strong oxidation ability, such as OH. The mechanism of RGO improving the photocatalytic activity is as follows. The chemical bonding interface between RGO and BiOCl can effectively reduce the energy barrier in the grain boundary region, promote electron transfer, and improve the separation efficiency of electrons and holes [38,39]. The electron has a very fast migration speed in graphene [40], so the chemical bonding interface between RGO and BiOCl can effectively reduce the energy barrier in the grain boundary region, promote electron transfer and improve the separation efficiency of electron-hole. The generated electrons combine with O and H to produce OH. The existence of holes can take away the electrons and OH⁻, and produce active free radicals with strong oxidation ability, such as OH. The corresponding photocatalytic properties are as follows:



Besides the above reason, RGO had the function of a large planar carrier, which could load BiOCl well and prevent polymerization. This means that the agglomeration of BiOCl could be significantly relaxed. As the result of the above reasons, the photocatalytic activity of BR was much better than that of the pure BiOCl. By the incorporation of PVP, the size of BiOCl was refined and the number of BiOCl adhered to the RGO was also significantly increased. And thus, the photocatalytic activity of BRP sample was the best among the three samples.

4. Conclusions

In summary, BiOCl/RGO and BiOCl/RGO-PVP photocatalysts were respectively prepared through a facile hydrothermal method. Some of the conclusions can be drawn as follows:

- (1) BiOCl were successfully synthesized in this work. However, the BiOCl were agglomerated into 3d flower-like microspheres in the pure BiOCl, while many of BiOCl were uniformly adhered onto RGO in the BiOCl/RGO. For the BiOCl/RGO-PVP sample, the BiOCl 3D flower-like microspheres were significantly refined and more BiOCl were adhered onto the surface of RGO.
- (2) The pure BiOCl showed a weak photocatalytic activity for the degradation of MO under visible light irradiation, with a rate constant of 0.03227 min⁻¹. The BiOCl showed an increased photocatalytic activity, with a rate constant of 0.04874 min⁻¹. The obtained BiOCl/RGO-PVP composite had the best photocatalytic activity, with a rate constant of 0.06205 min⁻¹.
- (3) The enhancement of the photocatalytic activity of the BiOCl/RGO was mainly attributed to the improved separation efficiency of

electrons-holes resulted from the addition of RGO and the formation of C-Bi bond. Adding PVP could refine the size of BiOCl and increased the number of BiOCl adhered onto RGO surfaces, thereby achieving the best photocatalytic activity.

Author contributions

F.Q. Li and B.H. Sun contributed equally to this work, and they conceived the idea and designed the experiments. Z.Y. Liu and X.Y. Liu performed the experiments. Y.L. Qin and B.H. Sun wrote the paper under the supervision of D.R. Ni and Z.Y. Ma. All authors participated in data analysis and discussion.

Declaration of competing interest

The authors declare that they have no known competing financial interests or personal relationships that could have appeared to influence the work reported in this paper.

Acknowledgments

The authors gratefully acknowledge the support of: (a) the program of Liaoning Education Department (No. LG201605), (b) Key Laboratory Open Fund of Shenyang Ligong University Nos. 4801004yb61-d and 4771004kfs49, (c) Key Research Program of Frontier Sciences, CAS (No. QYZDJ-SSW-JSC015) and (d) the Youth Innovation Promotion Association CAS (2020197).

References

- [1] J. Wang, C. Liu, S. Yang, X. Lin, W. Shi, Fabrication of a ternary heterostructure BiVO₄ quantum dots/C₆₀/g-C₃N₄ photocatalyst with enhanced photocatalytic activity, *J. Phys. Chem. Solid.* 136 (2020) 109164–109171.
- [2] Z. Zheng, W. Xie, B.B. Huang, Y. Dai, Plasmon-Enhanced solar water splitting on metal-semiconductor photocatalysts, *Chem. Eur J.* 24 (69) (2018) 18322–18333.
- [3] I.N. Reddy, C.V. Reddy, J. Shim, B. Akkinepally, M. Cho, K. Yoo, D. Kim, Excellent visible-light driven photocatalyst of (Al, Ni) co-doped ZnO structures for organic dye degradation, *Catal. Today* 340 (2020) 277–285.
- [4] M. Parthibavarman, M. Karthik, S. Prabhakaran, Facile and one step synthesis of WO₃ nanorods and nanosheets as an efficient photocatalyst and humidity sensing material, *Vacuum* 155 (2018) 224–232.
- [5] G.K. Upadhyay, J.K. Rajput, T.K. Pathak, V. Kumar, L.P. Purohit, Synthesis of ZnO:TiO₂ nanocomposites for photocatalyst application in visible light, *Vacuum* 160 (2019) 154–163.
- [6] Y.L. Qin, Z. Sun, W.W. Zhao, Z.Y. Liu, D.R. Ni, Z.Y. Ma, Improved photocatalytic properties of ZnS/RGO nanocomposites prepared with GO solution in degrading methyl orange, *Nano Struct. Nano Objects* 10 (2017) 176–181.
- [7] J.L. Song, Q.N. Fan, W.H. Zhu, R.F. Wang, Z.P. Dong, Preparation of BiOCl with high specific surface area and excellent visible light photocatalytic activity, *Mater. Lett.* 165 (2016) 14–18.
- [8] W. Liu, Y. Shang, A.N. Zhu, P. Tan, Y. Liu, L. Qiao, D. Chu, X. Xiong, J. Pan, Enhanced performance of doped BiOCl nanoplates for photocatalysis: understanding from doping insight into improved spatial carrier separation, *J. Mater. Chem. A* 24 (2017) 12542–12549.
- [9] C.Y. Wang, Y.J. Zhang, W.K. Wang, D.N. Pei, G.X. Huang, J.J. Chen, X. Zhang, H. Q. Yu, Enhanced photocatalytic degradation of bisphenol A by Co-doped BiOCl nanosheets under visible light irradiation, *Appl. Catal. B Environ.* 221 (2018) 320–328.
- [10] J.B. Pan, J.J. Liu, S.L. Zuo, A.K. Usman, Y.C. Yu, B.S. Li, Synthesis of cuboid BiOCl nanosheets coupled with CdS quantum dots by region-selective deposition process with enhanced photocatalytic activity, *Mater. Res. Bull.* 103 (2018) 216–224.
- [11] S.J. Wu, J.W. Xiong, J.G. Sun, D.H. Zachary, W. Zeng, Z.Z. Yang, L. Gu, X.X. Zhang, Y. Shize, Hydroxyl-dependent evolution of oxygen vacancies enables the regeneration of BiOCl photocatalyst, *ACS Appl. Mater. Interfaces* 19 (2017) 16620–16626.
- [12] J. Zhang, Z.W. Wang, M.G. Fan, P.P. Tong, J.Y. Sun, S.Y. Dong, J.H. Sun, Ultra-light and compressible 3D BiOCl/RGO aerogel with enriched synergistic effect of adsorption and photocatalytic degradation of oxytetracycline, *J. Mater. Res. Technol.* 8 (5) (2019) 4577–4587.
- [13] Y.L. Qin, Z. Sun, W.W. Zhao, Z.Y. Liu, D.R. Ni, Z.Y. Ma, Effect of S²⁻ donors on synthesizing and photocatalytic degrading properties of ZnS/RGO nanocomposite, *Appl. Phys. A Mater.* 123 (5) (2017) 355–360.
- [14] Suhee Kang, R.C. Pawar, Youngjun Pyo, Varsha Khare, Caroline Sunyong L, Size-controlled BiOCl-RGO composites having enhanced photodegradative properties, *J. Exp. Nanosci.* 11 (4) (2016) 259–275.

- [15] T. Chhabra, A. Kumar, A. Bahuguna, V. Krishnan, Reduced graphene oxide supported MnO₂ nanorods as recyclable and efficient adsorptive photocatalysts for pollutants removal, *Vacuum* 160 (2019) 333–346.
- [16] M. Sharma, K. Behl, S. Nigam, M. Joshi, TiO₂-GO nanocomposite for photocatalysis and environmental applications: a green synthesis approach, *Vacuum* 156 (2018) 434–439.
- [17] H. Liu, T. Lv, X.H. Wu, C.K. Zhu, Z.F. Zhu, Preparation and enhanced photocatalytic activity of CdS@RGO core-shell structural microspheres, *Appl. Surf. Sci.* 305 (2014) 242–246.
- [18] P. Wang, J. Wang, X.F. Wang, H.G. Yu, J.G. Yu, M. Lei, Y.G. Wang, One-step synthesis of easy-recycling TiO₂-rGO nanocomposite photocatalysts with enhanced photocatalytic activity, *Appl. Catal. B Environ.* 132 (2013) 452–459.
- [19] H. Zhao, X. Liu, Y. Dong, Y.M. Xia, H.J. Wang, X.M. Zhu, Fabrication of a Z-scheme (001)/(110) facet heterojunction in BiOCl to promote spatial charge separation, *ACS Appl. Mater. Interfaces* 12 (28) (2020) 31532–31541.
- [20] Y.H. Ren, J.H. Zou, K.Q. Jing, Y.Y. Liu, B.B. Guo, Y.J. Song, Y. Yu, Ling Wu, Photocatalytic synthesis of N-benzylethylamine from benzylamine on ultrathin BiOCl nanosheets under visible light, *J. Catal.* 380 (2020) 123–131.
- [21] S. Araki, K. Nakanishi, A. Tanaka, H. Kominami, A ruthenium and palladium bimetallic system superior to a rhodium co-catalyst for TiO₂-photocatalyzed ring hydrogenation of aniline to cyclohexylamine, *J. Catal.* 389 (2020) 212–217.
- [22] G. Greczynski, L. Hultman, X-ray photoelectron spectroscopy: towards reliable binding energy referencing, *Prog. Mater. Sci.* 107 (2020) 100591.
- [23] G. Greczynski, L. Hultman, C 1s peak of adventitious carbon aligns to the vacuum level: dire consequences for material's bonding assignment by photoelectron spectroscopy, *ChemPhysChem* 18 (2017) 1507–1512.
- [24] G. Greczynski, L. Hultman, Compromising science by ignorant instrument calibration- need to revisit half a century of published XPS data, *Angew. Chem. Int. Ed.* 59 (2020) 5002–5006.
- [25] G. Greczynski, L. Hultman, Reliable determination of chemical state in x-ray photoelectron spectroscopy based on sample-work-function referencing to adventitious carbon: resolving the myth of apparent constant binding energy of the C 1s peak, *Appl. Surf. Sci.* 451 (2018) 99–103.
- [26] X. Yu, J.J. Shi, L.J. Feng, C.H. Li, L. Wang, A three-dimensional BiOBr/RGO heterostructural aerogel with enhanced and selective photocatalytic properties under visible light, *Appl. Surf. Sci.* 396 (2017) 1775–1782.
- [27] Y.Q. Yang, W.K. Zhang, R.X. Liu, J.M. Cui, C. Deng, Preparation and photocatalytic properties of visible light driven Ag-AgBr-RGO composite, *Separ. Purif. Technol.* 190 (2018) 278–287.
- [28] J.L. Hu, X. Wu, C.J. Huang, W.J. Fan, X.Q. Qiu, Visible light photocatalytic activity induced by Rh(III) modification on the surface of BiOCl, *Appl. Surf. Sci.* 387 (2016) 45–50.
- [29] L. Li, M.Y. Zhang, Y. Liu, X.T. Zhang, Hierarchical assembly of BiOCl nanosheets onto bicrystalline TiO₂ nanofiber: enhanced photocatalytic activity based on photoinduced interfacial charge transfer, *J. Colloid Interface Sci.* 435 (2014) 26–33.
- [30] M.S. Zhu, P.L. Chen, M.H. Liu, Ag/AgBr/graphene oxide nanocomposite synthesized via oil/water and water/oil microemulsions: a comparison of sunlight energized plasmonic photocatalytic activity, *Langmuir* 28 (2012) 3385–3390.
- [31] H. Wang, Y.H. Liang, L. Liu, J.S. Hu, P. Wu, W.Q. Cui, Enriched photoelectrocatalytic degradation and photoelectric performance of BiOI photoelectrode by coupling rGO, *Appl. Catal. B Environ.* 208 (2017) 22–34.
- [32] L.H. Tian, J.Y. Liu, C.Q. Gong, L.Q. Ye, L. Zan, Fabrication of reduced graphene oxide-BiOCl hybrid material via a novel benzyl alcohol route and its enhanced photocatalytic activity, *J. Nanoparticle Res.* 15 (9) (2013) 1917–1927.
- [33] S. Kang, R.C. Pawar, Y. Pyo, V. Khare, C.S. Lee, Size-controlled BiOCl-RGO composites having enhanced photodegradative properties, *J. Exp. Nanosci.* 11 (4) (2016) 259–275.
- [34] Y.L. Zhang, D.Y. Li, Y.G. Zhang, X.F. Zhou, S.J. Guo, L.B. Yang, Graphene-wrapped Bi₂O₂CO₃ core-shell structures with enhanced quantum efficiency profit from an ultrafast electron transfer process, *J. Mater. Chem. A.* (2) (2014) 8273–8280.
- [35] J. Wu, B.B. Liu, Z.X. Ren, M.Y. Ni, C. Li, Yi Y. Gong, W. Qin, Y.L. Huang, C.Q. Sun, X.J. Liu, CuS/RGO hybrid photocatalyst for full solar spectrum photoreduction from UV/Vis to near-infrared light, *J. Colloid Interface Sci.* 517 (2018) 80–85.
- [36] J.F. Niu, P.X. Dai, Q. Z. B.H. Yao, X.J. Yu, Microwave-assisted solvothermal synthesis of novel hierarchical BiOI/rGO composites for efficient photocatalytic degradation of organic pollutants, *Appl. Surf. Sci.* 430 (2018) 165–175.
- [37] K.S. Divya, Akash Chandran, V.N. Reethu, Suresh Mathew, Enhanced photocatalytic performance of RGO/Ag nanocomposites produced via a facile microwave irradiation for the degradation of Rhodamine B in aqueous solution, *Appl. Surf. Sci.* 444 (2018) 811–818.
- [38] Z.J. Li, Y. Qu, K. Hu, M. Humayun, S.Y. Chen, L.Q. Jing, Improved photoelectrocatalytic activities of BiOCl with high stability for water oxidation and MO degradation by coupling RGO and modifying phosphate groups to prolong carrier lifetime, *Appl. Catal. B Environ.* 203 (2017) 355–362.
- [39] X.K. Zheng, J.J. Yuan, J. Shen, J.X. Liang, J.F. Che, B. Tang, G.Y. He, H.Q. Chen, A carnation-like rGO/Bi₂O₂CO₃/BiOCl composite: efficient photocatalyst for the degradation of ciprofloxacin, *J. Mater. Sci. Mater. Electron.* 30 (6) (2019) 5986–5994.
- [40] Y.L. Qin, W.W. Zhao, Z. Sun, X.Y. Liu, G.L. Shi, Z.Y. Liu, D.R. Ni, Z.Y. Ma, Photocatalytic and adsorption property of ZnS-TiO₂/RGO ternary composites for methylene blue degradation, *Adsorpt. Sci. Technol.* 37 (2019) 764–776.